Role of Substrate Material in Failure of Crown-Like Layer Structures

Jae-Won Kim,* Sanjit Bhowmick, Herzl Chai, Brian R. Lawn

Materials Science and Engineering Laboratory, National Institute of Standards and Technology, Gaithersburg, Maryland 20899-8500

Received 24 February 2006; revised 1 June 2006; accepted 6 June 2006
Published online 4 October 2006 in Wiley InterScience (www.interscience.wiley.com). DOI: 10.1002/jbm.b.30666

Abstract: The role of substrate modulus on critical loads to initiate and propagate radial cracks to failure in curved brittle glass shells on compliant polymeric substrates is investigated. Flat glass disks are used to drive the crack system. This configuration is representative of dental crown structures on dentin support in occlusal contact. Specimens are fabricated by truncating glass tubes and filling with epoxy-based substrate materials, with or without alumina filler for modulus control. Moduli ranging from 3 to 15 GPa are produced in this way. Critical loads for both initiation and propagation to failure increase monotonically with substrate modulus, by a factor of two over the data range. Fracture mechanics relations provide a fit to the data, within the scatter bands. Finite element analysis is used to determine stress distributions pertinent to the observed fracture modes. It is suggested that stiffer substrate materials offer potential for improved crown lifetime in dental practice. © 2006 Wiley Periodicals, Inc.† J Biomed Mater Res Part B: Appl Biomater 81B: 305–311, 2007

Keywords: **curved surfaces; radial cracks; contact damage; brittle shells; dental crowns**

INTRODUCTION

Layer structures with hard, brittle coatings on compliant substrates are evident in many engineering applications. Many studies have been carried out on flat brittle ceramic layers on compliant substrates in concentrated surface loading.[1–3] The prototypical model system is that of a flat glass plate (Young's modulus ~70 GPa) bonded to a polycarbonate or epoxy base (modulus ~3 GPa) with a thin layer of adhesive, indented at the top surface with a hard sphere.[4] Transparency in both layers enables direct observation of fracture evolution, from initiation to failure. Of several fracture modes reported, radial cracking originating at the bottom surface of the brittle layer (i.e., at the interlayer interface) is the most deleterious, especially in thinner brittle layers, because of its capacity to extend readily to component boundaries.

Studies of such brittle-layer systems are especially relevant to all-ceramic dental crowns on tooth dentin, which are subject to occlusal contact forces and thus to premature *in vivo* failure.[5–11] An important element of the occlusal contact is curvature of the crown surface. Recent studies on curved glass/polycarbonate bilayers have revealed some new features in radial fracture patterns, most notably in the conditions of final failure.[12–14] In those studies, specimens were prepared by allowing originally flat glass plates to slump over a ball at the softening temperature. Epoxy resin was poured into the cooled shells, producing dome-like bilayer structures. Indentation either with spheres or flat disks (inverted Hertzian test) of various moduli promoted failure by propagation of radial cracks from the near-contact zones to the dome bases. Surface-initiated cone cracks were found to play a subsidiary role in the failure process in the thin-layer systems of interest here.

In the present paper we take the study of curved surfaces one step further, by investigating the role of substrate modulus on the failure condition. Such a study is of interest in the clinical context because of the practical possibility of replacing tooth dentin (modulus ~16 GPa) with stiffer support "buildup" material. There is precedent in some flat-layer studies indicating that higher substrate modulus may significantly inhibit radial fracture.[15,16] In this context, the simple polycarbonate or epoxy substrates used in our preceding model experiments may be regarded as restrictive, because of their comparatively low stiffness. Accordingly, we carry out tests on curved specimens filled with both epoxy and particulate-filled polymer composites, covering a range of substrate moduli between 3 and 15 GPa. We prepare the specimen shells in a somewhat different way to before, this time by cutting the ends of glass test tubes so as to leave dome with a residual cylindrical base. Indenta-

Correspondence to: B. R. Lawn (e-mail: brian.lawn@nist.gov)
*Present address: Department of Biomaterials and Biomimetics, College of Dentistry, New York University, New York, NY 10010
Contract grant sponsor: U.S. National Institute of Dental and Craniofacial Research; contract grant sponsor: PO1 DE10976.

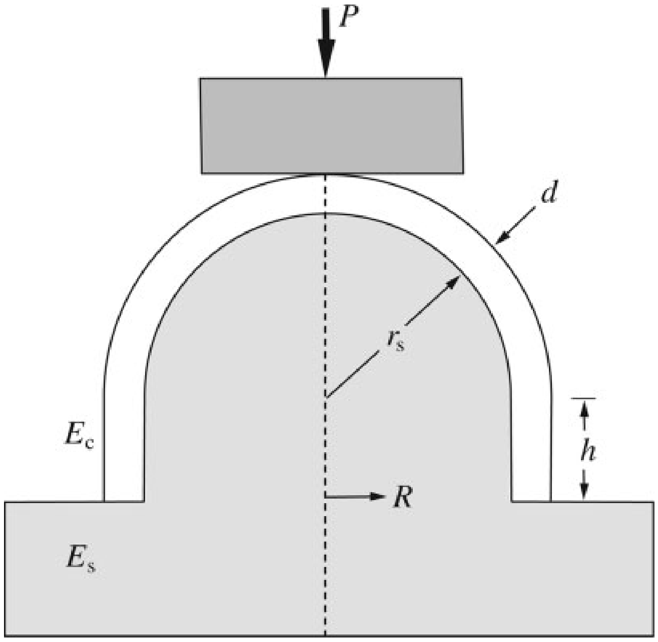

Figure 1. Schematic showing specimen and contact testing parameters. Glass test tube of thickness d and inner radius $r_s = 4$ mm is cut off with axial height $h = 6$ mm, filled with polymer-based material as substrate, and bonded to base of same material as substrate. Indenter is flat glass disk.

tion is carried out by loading with a glass disk, in simulation of occlusal contacts with like modulus (e.g. tooth enamel on veneered porcelain crown), and the evolution of radial fracture is followed from initiation to failure. Basic fracture mechanics and finite element analyses are used to interpret the results.

EXPERIMENTAL METHODS

Specimen Fabrication

The experimental setup is depicted in the schematic of Figure 1. Commercially available glass tubes of inner radius $r_s = 4$ mm and wall thickness $d = 0.6$ mm, modulus $E_c = 70$ GPa (Fisherbrand, Fisher Scientific, USA), were cut 6 mm below the dome equator to simulate the cylindrical wall of a domed crown structure. The glass surfaces were etched to remove spurious flaws (10% HF, 1 min). The interior walls in the hemispherical region were then abraded with a slurry of 600 grade SiC grit to introduce controlled flaws for starting radial cracks.[4] This simulates the sandblasting treatment given to the undersurfaces of all-ceramic crowns in clinical practice.[17]

An epoxy resin (Harcos Chemicals, Bellesville, NJ) was used as a base polymeric filler material. By mixing with different amounts of hardener, 16% and 33% by weight, the base modulus could be varied. Stiffer composites were fabricated by adding 0.3 μm alumina powder (AKP-30, Sumitomo Co, Japan) in amounts of 20 and 40% by weight to the epoxy mix with less hardener, and mixed for 12 h before curing. The mixes were poured into dummy glass tubes as molds and were then allowed to cure for 48 h at room temperature. Substrates of four different moduli were thereby produced. These moduli, measured using the Oliver and Pharr nanoindentation method,[18] are indicated in Table I. The filler material tended to shrink during curing, causing some of the molds to fracture spontaneously. Those molds that did not fracture were broken open to remove the polymer plugs. The plugs were then polished and reinserted into the actual test shells, using the same resin material to fill the gaps and to bond the plugs to the glass walls. The resultant structures were then bonded onto support bases of thickness 4 mm, again of the same resin material (Figure 1).

TABLE I. Elastic Constants for Materials Used in This Study

Material	Young's Modulus (GPa)
Glass	70
Soft epoxy (16% hardener)	3.0
Hard epoxy (33% hardener)	4.1
Soft composite (20% alumina)	9.3
Hard composite (40% alumina)	15.0

Failure Testing

The test specimens were loaded with a flat glass disk indenter 5 mm thick and 10 mm diameter. The flat provided an inverted Hertzian contact with simple axial alignment. Tests were made on a screw-driven testing machine (Instron 5500R, Instron Corp, Canton MA), at peak loads up to $P = 1000$ N. Video cameras were used to record radial crack evolution during testing, with back lighting to illuminate the cracks.[12] This required careful positioning of the cameras, particularly in the earlier phases of fracture where the indenter tended to obscure the near-contact regions. Crack initiation was measured from below the specimen as the load P_I at which the radial cracks abruptly appeared.[4] Failure was measured as the load P_F at which radial cracks penetrated from the subsurface to the outer glass dome surface at a location of about 30° relative to the load axis, at which point they became unstable and ran to the cylindrical base.[12] Each critical event was confirmed by small signature drops in the load versus crosshead-displacement records. Continuation of loading led to crushing of the shell, marked by a much higher load drop. Even at this point, the inner polymeric support continued to support about 60% of the peak load.

Some failed specimens were sectioned through the load axis to shed further light on the failure modes. The cut sections were polished to a 1 μm diamond finish and lightly etched to highlight the cracks.[19]

RESULTS

Fracture Morphology

Figure 2 shows radial crack configurations in two glass shell specimens containing substrate fillers at extremes of the modulus range in Table I: (a) modulus $E_s = 3.0$ GPa,

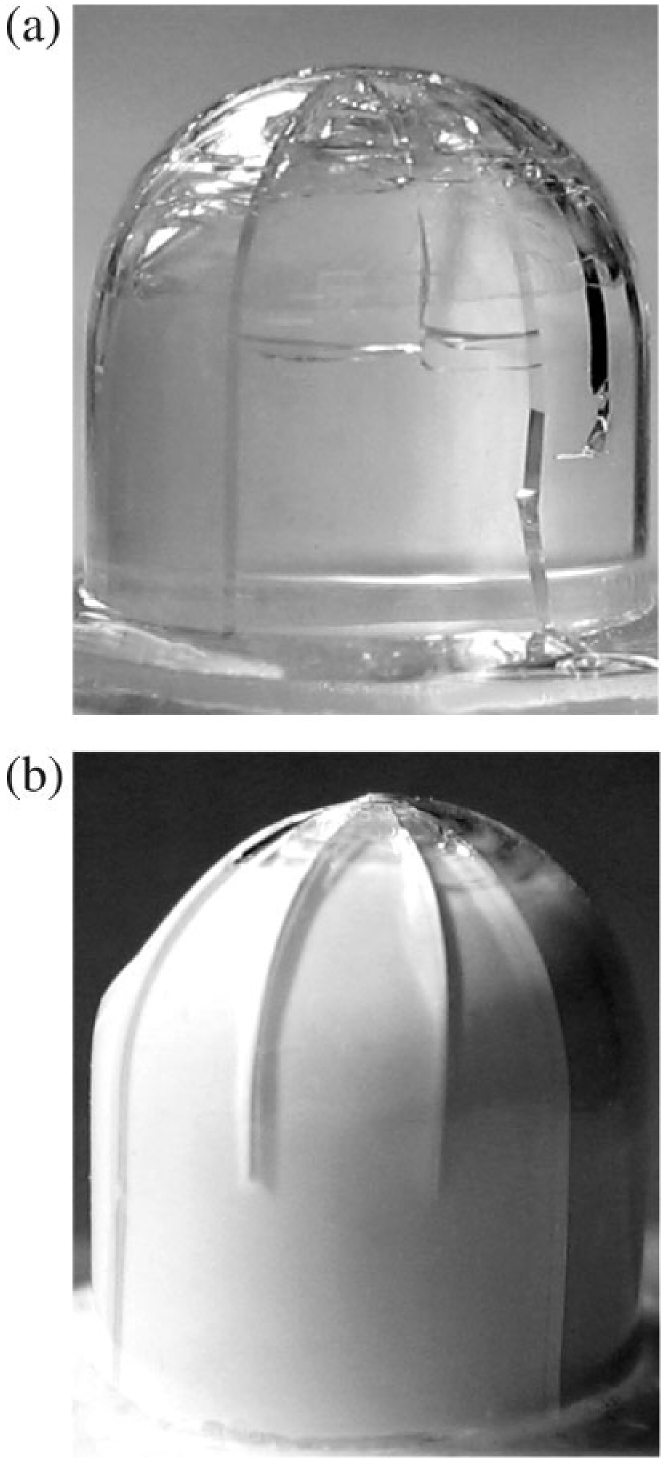

Figure 2. Glass dome structures indented with glass disks of modulus $E_c = 70$ GPa but with different substrate modulus E_s, at loads P about 10% higher than that required to cause failure: (a) $E_s = 3$ GPa, $P = 750$ N; (b) $E_s = 15$ GPa, $P = 820$ N. Several radial cracks have extended to tube margins. Some additional cone crack damage is observed in contact region.

(b) $E_s = 15$ GPa. The photographs represent overload configurations beyond failure in which the load has dropped abruptly by $\sim$40%. The most significant feature in the photographs is the appearance of radial cracks extending from the contact zone to the specimen bases. The lead radial cracks initiated at relatively small loads, propagated stably around the dome shoulder, and there propagated rapidly to failure. Some radial cracks have arrested part way down the cylindrical base.

Also evident in Figure 2 is some additional circumferential cracking and spalling in the near-contact region. These cracks have linked up with the foregoing radials to produce dislodging segments, so that the protective brittle shell no longer supports the bulk of the applied loading.[12] This incidence of spalling accounts for the substantial load drop. To obtain a clearer view of this overload state, Figure 3 shows a section view of the upper dome region of a specimen taken under the same conditions as that in Figure 2(a). A radial crack is evident as the vertical trace extending through the specimen thickness along the contact axis. Cone cracks have extended within the shell from the near-contact, spreading laterally and intersecting the inner and outer surfaces in the shoulder regions into the circumferential crack patterns. At this point gross spalls have occurred and the crown-like structure is on the verge of disintegration.

Critical Loads

Figure 4 plots critical loads P_I for initiation and P_F for failure as a function of modulus ratio E_s/E_c ($E_c = 70$ GPa = constant). Data points are means and standard deviations of a minimum six tests per specimen. Note the near order-of-magnitude "window" between P_I and P_F, representing the period of stable crack growth between initiation and failure as the radial crack propagates from the near-contact zone around the dome shoulder. A systematic rise in both P_I and P_F with increasing E_s is apparent, amounting to a factor of almost two over the modulus range covered, attesting to the benefits of a stiffer substrate beneath the brittle shell.

The solid lines in Figure 4 are fits to the data using fracture mechanics relations for a specimen of thickness d:[14]

$$P_I = BSd^2/\log(E_c/E_s) \tag{1a}$$

$$P_F = B'K_c d^{3/2}/\log(E_c/E_s) \tag{1b}$$

where S is the strength and K_c the toughness of the brittle layer, and B and B' are geometrical parameters which depend on inner dome radius r_s. The initiation relation

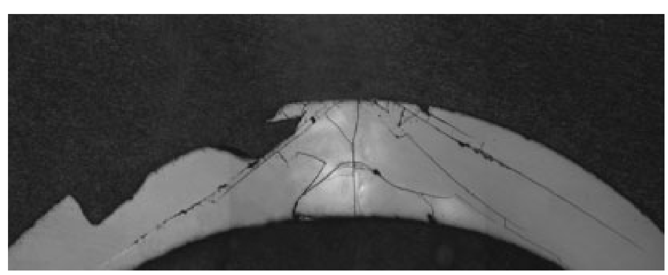

Figure 3. Section and etch profile of failed glass tube specimen filled with substrate of modulus $E_s = 15$ GPa, at $P = 820$ N. Traces of radial cracks and cone cracks, with extensive spalling, are apparent.

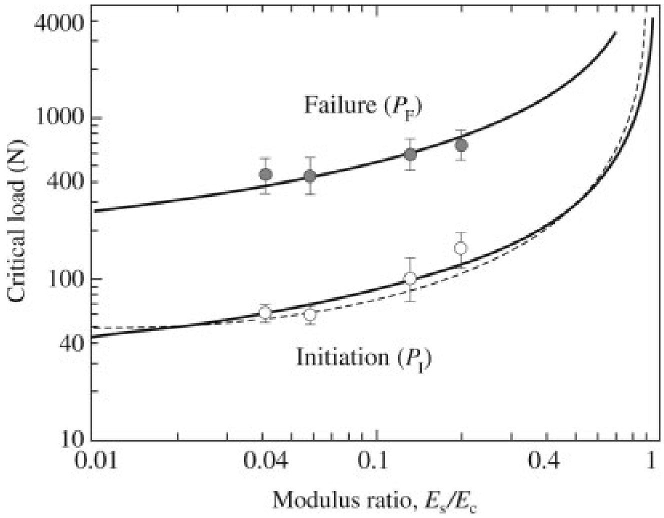

Figure 4. Critical loads P_I and P_F for initiation (unfilled symbols) and failure (filled symbols) of filled glass tubes indented with glass disks, as function of modulus mismatch E_s/E_c. Experimental points are means and standard deviations. Solid lines are fits to fracture mechanics relations for P_I and P_F. Dashed line is FEA prediction for P_I.

Eq. (1a) is derived from the theory of plates on semi-infinite compliant supports in concentrated loading,[20] equating the maximum tensile stress at the brittle layer undersurface to the material strength and adjusting the dimensionless coefficient B using finite element analysis (FEA).[21] The failure relation Eq. (1b) is based on a rigorous boundary element analysis (BEA) of radial fracture in curved shells,[14] following on from an earlier FEA study on flat layers by Cao,[22] in which the evolving crack geometry and corresponding stress intensity factors are computed stepwise through to full penetration onto the shoulder of the shell surface at about 30° to the load axis. This point of penetration coincides with the onset of crack instability.[14] The fits are within the scatter in data. Note the explicit logarithmic dependence of P_I and P_F on the modulus mismatch ratio E_s/E_c. This dependence arises from the theory of plates on semi-infinite compliant supports in concentrated loading,[20] and so strictly applies only within the limit $d \ll r_s$. The data fits are made by inserting $d = 0.6$ mm into Eq. (1) and adjusting $BS = 240$ MPa and $B'K_c = 36$ MPa m$^{1/2}$. If we take $B = 2.0$ from a previous study,[21] we obtain $S = 120$ MPa, which is close to the reported strength of abraded glass, corresponding to a flaw size of about 10 μm.[4] (For the layer thickness 0.6 mm used here, the flaw size is sufficiently small that size effects in the strength of the glass may be neglected.[23]) If we take $K_c = 0.6$ MPa m$^{1/2}$ for glass,[24] we obtain $B' = 60$.

FINITE ELEMENT ANALYSIS

FEA Code

Finite element analysis (FEA) with ANSYS software (Version 6.0, ANSYS, Cannonsburg, PA) was used to calculate relevant pre-crack stresses in the axisymmetrically-loaded dome-shaped bodies. The code was similar to that previously described for sphere indentation on flat bilayers, but now with the specimen geometry of Figure 1.[25,26] Specimen dimensions were the same as those used experimentally, and input moduli are those listed in Table I (with Poisson's ratio 0.22 for glass and 0.35 for the polymer-based substrates). The contact was assumed to be frictionless, the deformations everywhere elastic, and the shell/substrate interface well bonded. Grid spacings were refined until convergence was attained in test runs, with more than 10^4 total elements.

The stresses of primary interest were axial compression stresses in the shell and substrate, and hoop tensile stresses in the shell, the first to ascertain how the applied load is partitioned between the shell and substrate and the second to determine the distribution of crack driving stresses perpendicular to the radial crack plane.

Stress Distributions

The FEA computations can be used to validate Eq. (1a) for radial crack initiation by determining, for any given substrate, the critical load P_I at which the maximum hoop tensile stress along the contact axis at the glass shell undersurface equals the strength $S = 120$ MPa.[27] The prediction from such computations is plotted as the dashed line in Figure 4. The broad trend mirrors that of the solid line representation of Eq. (1a), notwithstanding deviations of up to 10% over the data range.

Analogous predictions of the critical load P_F for failure are not so straightforward, requiring incorporation of a well-developed radial crack into the FEA algorithm, with constant remeshing at each crack increment, as mentioned in connection with Eq. (1b).[14] Nevertheless, the distributions of pre-crack stresses within the dome structure serve to indicate the load partitioning between shell and substrate. Figures 5–7 plot these distributions for two E_s/E_c values, (a) = 0.03 and (b) 0.3 (embracing the data range in Figure 4). In such plots it is convenient to normalize all stresses to the mean pressure $p_m = P/\pi(r_s + d)^2$ at the cylindrical base of the composite specimen (shell plus substrate), noting a certain geometrical similarity in the elastic stress fields for ideally concentrated loads (contact radius $\ll$ shell thickness d). Such "point load" conditions are reasonably well approximated in the loading configurations under consideration here.

Figure 5 plots normalized axial compression stress contours in both shells and substrates. This plot demonstrates how the structure supports the applied load for different E_s/E_c. Generally, whereas the higher stresses are concentrated in the near-contact regions, the load is borne more uniformly near the cylindrical base regions. To emphasize this last point, Figure 6 plots this axial stress component as a function of normalized distance $R/(r_s + d)$ measured along a base radius from the contact axis for each substrate (Figure 1).

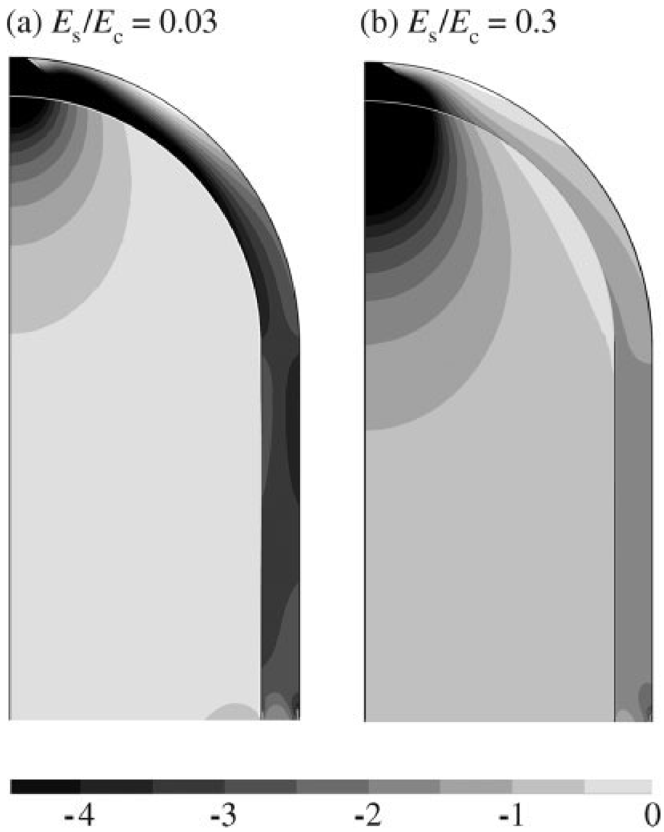

Figure 5. Contours of compressive axial stresses in glass of modulus E_c = 70 GPa and in substrate, for (a) E_s = 2 GPa and (b) E_s = 20 GPa. Stresses normalized to mean pressure p_m at base of filled shell.

(Actually, the stresses in this plot are measured 1 mm above the base to avoid stress singularities at the shell corners.) The dashed line in Figure 6 represents the mean pressure. The important feature of note here is the reduced percentage of applied load borne by the shell with the relatively stiffer substrate: i.e., 48% for $E_s/E_c = 0.3$ compared to 69% for $E_s/E_c = 0.03$. This partitioning is reflected in the lower intensity of stress contours within the shell in Figure 5(b) relative to Figure 5(a).

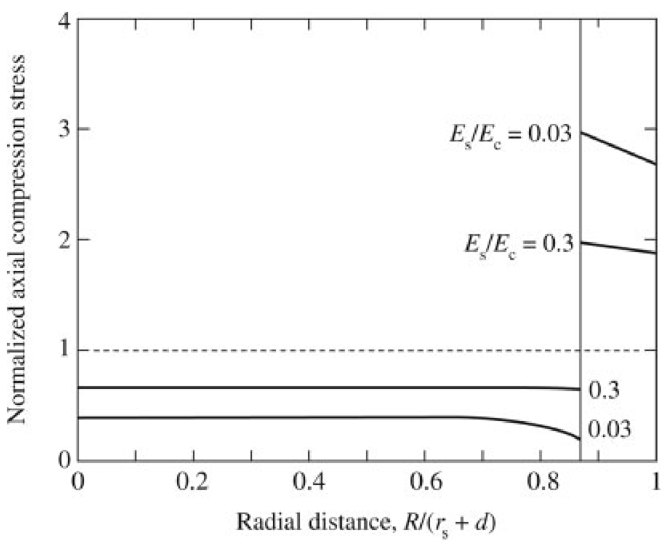

Figure 6. Plot of normalized compression stress along base of filled shell. Vertical line indicates substrate/shell interface. Horizontal dashed line is mean pressure.

Figure 7 plots tensile hoop tension stress contours in the shells responsible for driving the radial cracks. In both cases shown the tensile stresses spread around the dome onto the shoulder regions, where crack instability to failure occurs. The stress intensity in the structure with stiffer substrate has substantially less intense hoop stress contours in the shoulder region. This means that a higher applied load is required to drive the stiffer-substrate system to failure, accounting for the rising $P_F(E_s/E_c)$ dependence in Figure 4. Note also the slow stress gradients in this shoulder region, accounting for the instability in crack growth once the radials penetrate to the outer glass surface.[14]

DISCUSSION

The chief finding of this study is confirmation of the role of substrate modulus (E_s) on the critical loads for cracking, both initiation (P_I) and propagation (P_F), in brittle crown-like shell structures. In Figure 4, P_I and P_F increase by a factor of about 2 over a range of 5 in E_s. These results are consistent with the simple logarithmic dependence on E_s/E_c

Figure 7. Contours of hoop tensile stresses in glass shell of modulus E_c = 70 GPa, for substrate modulus (a) E_s = 2 GPa and (b) E_s = 20 GPa. Stresses normalized to mean pressure p_m at base of filled shell.

in Eq. (1). Physically, such gains are attributable to suppression of flexural tensile stresses in the brittle shell layer by the stiffer support. The results in Figure 4 also suggest that more substantial increases in P_I and P_F might be realized by using even stiffer substrates, e.g. in the form of high modulus "buildup" materials in clinical preparation for crown placement. At the same time, care would need to be exercised to ensure that any such additional support does not come at the expense of compromising the composite crown/tooth structure, acknowledging that stiffer substrate materials will most certainly bear more of the occlusal load and might themselves be prone to fracture.

The principal mode of failure in the tests conducted here is that of radial fracture. There is evidence in the literature to suggest that this mode is the one most responsible for the failure of all-ceramic dental crowns.[6,7,11] The radial cracks initiate and pop in below the contact at the undersurface of the glass dome at load P_I, spread outward through the shell thickness and onto the dome shoulders with increasing P, and ultimately run downward to failure at the cylindrical base at load P_F. At even higher loads, cone cracks link up with the radials and spall triangular segments, greatly diminishing the system compliance and transferring the load to the substrate.[12] Cone cracks are likely to become more dominant in specimens with greater thickness,[28] in specimens with higher curvature (less distance to travel before intersection with shell walls), in cyclic loading in liquids where hydraulic forces act preferentially to drive surface fractures,[29,30] and in contacts with small spherical indenters (more concentrated contacts—see later).[31]

The properties of the brittle shell as well as the substrate warrant comment here. The appearance of strength S in Eq. (1a) in place of toughness K_c in Eq. (1b) reflects a basic difference in the instability condition: initiation occurs at a critical stress from a pre-existing flaw, more or less independent of specimen dimension; failure occurs when the radial crack reaches a critical location on the dome shoulder, independent of surface flaw size. Hence it is only P_I, and not P_F, that is sensitive to flaw size. This means that improvement in crown preparation to avoid severe flaws (e.g. by restricting sandblast treatments) may help to suppress initiation of radial cracks, but will be of little use in containing any such cracks once they form. It is possible in some cases for P_I to be so high as to exceed P_F, e.g. in highly curved shells with unabraded or (especially) etched surfaces, so that initiation leads spontaneously to failure.[32]

Other, geometrical factors also require consideration. We have tested glass tubes of relatively small wall thickness in the clinical context, $d = 0.6$ mm. As far as radial fracture is concerned, this focus on one small wall thickness is hardly restrictive, because of the explicit d dependence in Eq. (1)—extrapolating to thicker specimens is a simple scaling exercise. We have also considered only glass disk indenters. Note that there is no indication of contact dimension in Eq. (1), consistent with a dominant flexural mode for radial cracking, i.e. independent of local Hertzian stresses. The condition for Eq. (1) to remain valid is that the contact dimension should be small relative to d, which is generally the case as long as the indenter is as least as hard as the shell material and the loads are not too high. This condition can change in contacts with ultra-compliant indenters (e.g., food bolus) where the brittle shell undersurfaces become engulfed within a rapidly spreading compressive zone. In such cases the tensile stress concentrations shift around the dome shoulders toward the margins, and can promote edge failures.[33] We have already mentioned that replacement of a disk indenter with a small sphere, while not significantly altering the radial fracture mechanics, may promote cone cracking as another mode of failure.

Finally, some limitations in the fracture mechanics analyses may be acknowledged. (i) *Assumptions in fracture mechanics*. Equation (1) is derived from the theory of flat plates on semi-infinite compliant supports. Such theory is the basis of the logarithmic term in E_s/E_c. Note, however, that $P_I \rightarrow 0$ and $P_F \rightarrow 0$ in Eqs. (1a) and (1b) when $E_s/E_c \rightarrow 0$, which cannot be true for curved surfaces in Figure 1, because in those cases the margins will still support some load prior to failure. The deviations between the predictions of Eq. (1a) and the FEA computations for P_I in Figure 4 also point to the approximate nature of the fracture mechanics. (ii) *Departures from elasticity*. We have assumed perfectly elastic deformation. Some plastic deformation may be possible in some substrates. Based on estimates of substrate yield stresses σ_Y from the simple relation $\sigma_Y = H/3$, where H is hardness,[34] our materials did not enter this region. However, such yield has been observed in bilayers with metal substrates, with consequent enhancement of flexural stresses and hence premature radial cracking.[35] (iii) *Geometrical similarity*. We have assumed point loading in the contact at the shell surface. We have already mentioned likely breakdown of this assumption when the indenter is much more compliant than the shell material, leading not only to suppression of flexural tensile stresses but also a potential change in fracture mode.

REFERENCES

1. Lawn BR. Ceramic-based layer structures for biomechanical applications. Curr Opin Solid State Mater Sci 2002;6:229–235.
2. Lawn BR, Deng Y, Miranda P, Pajares A, Chai H, Kim DK. Overview: Damage in brittle layer structures from concentrated loads. J Mater Res 2002;17:3019–3036.
3. Deng Y, Lawn BR, Lloyd IK. Characterization of damage modes in dental ceramic bilayer structures. J Biomed Mater Res 2002;63:137–145.
4. Chai H, Lawn BR, Wuttiphan S. Fracture modes in brittle coatings with large interlayer modulus mismatch. J Mater Res 1999;14:3805–3817.
5. McLean JW.The Science and Art of Dental Ceramics, Vol. 1: The Nature of Dental Ceramics and Their Clinical Use. Chicago: Quintessence; 1979.

6. Kelly JR. Ceramics in restorative and prosthetic dentistry. Annu Rev Mater Sci 1997;27:443–468.
7. Kelly JR. Clinically relevant approach to failure testing of all-ceramic restorations. J Prosthet Dent 1999;81:652–661.
8. Malament KA, Socransky SS. Survival of dicor glass-ceramic dental restorations over 14 years. I. Survival of dicor complete coverage restorations and effect of internal surface acid etching, tooth position, gender and age. J Prosthet Dent 1999; 81:23–32.
9. Malament KA, Socransky SS. Survival of dicor glass-ceramic dental restorations over 14 years. II. Effect of thickness of dicor material and design of tooth preparation. J Prosthet Dent 1999;81:662–667.
10. Malament KA, Socransky SS. Survival of dicor glass-ceramic dental restorations over 16 years, Part III: Effect of luting agent and tooth or tooth-substitute core structure. J Prosthet Dent 2001;86:511–519.
11. Lawn BR, Deng Y, Thompson VP. Use of contact testing in the characterization and design of all-ceramic crown-like layer structures: A review. J Prosthet Dent 2001;86:495–510.
12. Qasim T, Bush MB, Hu X, Lawn BR. Contact damage in brittle coating layers: Influence of surface curvature. J Biomed Mater Res B 2005;73:179–185.
13. Qasim T, Ford C, Bush MB, Hu X, Lawn BR. Effect of off-axis concentrated loading on failure of curved brittle layer structures. J Biomed Mater Res B 2006;76:334–339.
14. Rudas M, Qasim T, Bush MB, Lawn BR. Failure of curved brittle layer systems from radial cracking in concentrated loading. J Mater Res 2005;20:2812–2819.
15. Scherrer SS, deRijk WG. The fracture resistance of all-ceramic crowns on supporting structures with different elastic moduli. Int J Prosthodont 1993;6:462–467.
16. Lee KS, Rhee Y-W, Blackburn DH, Lawn BR, Chai H. Cracking of brittle coatings adhesively bonded to substrates of unlike modulus. J Mater Res 2000;15:1653–1656.
17. Zhang Y, Lawn BR, Rekow ED, Thompson VP. Effect of sandblasting on the long-term strength of dental ceramics. J Biomed Mater Res B 2004;71:381–386.
18. Oliver WC, Pharr GM. An improved technique for determining hardness and elastic-modulus using load and displacement sensing indentation experiments. J Mater Res 1992;7:1564–1583.
19. Mikosza AG, Lawn BR. Section-and-etch study of hertzian fracture mechanics. J Appl Phys 1971;42:5540–5545.
20. Timoshenko S, Woinowsky-Krieger S. Theory of Plates and Shells. New York: McGraw-Hill; 1959.
21. Rhee Y-W, Kim H-W, Deng Y, Lawn BR. Contact-induced damage in ceramic coatings on compliant substrates: Fracture mechanics and design. J Am Ceram Soc 2001;84: 1066–1072.
22. Cao YQ. Three-dimensional finite element modeling of subsurface median crack in trilayer sandwiches due to contact loading. Eng Fract Mech 1996;69:729–743.
23. Chai H. Crack propagation in glass coatings under expanding spherical contact. J Mech Phys Solids 2006;54:447–466.
24. Wiederhorn SM. Fracture surface energy of glass. J Am Ceram Soc 1969;52:99–105.
25. Chai H, Lawn BR. Cracking in brittle laminates from concentrated loads. Acta Mater 2002;50:2613–2625.
26. Chai H, Lawn BR. Fracture mode transitions in brittle coating layers on compliant substrates as a function of thickness. J Mater Res 2004;19:1752–1761.
27. Kim H-W, Deng Y, Miranda P, Pajares A, Kim DK, Kim H-E, Lawn BR. Effect of flaw state on the strength of brittle coatings on soft substrates. J Am Ceram Soc 2001;84:2377–2384.
28. Chai H. Transverse fracture in thin-film coatings under spherical indentation. Acta Mater 2005;53:487–498.
29. Kim DK, Jung Y-G, Peterson IM, Lawn BR. Cyclic fatigue of intrinsically brittle ceramics in contact with spheres. Acta Mater 1999;47:4711–4725.
30. Zhang Y, Kwang J-K, Lawn BR. Deep penetrating conical cracks in brittle layers from hydraulic cyclic contact. J Biomed Mater Res B 2005;73:186–193.
31. Rhee Y-W, Kim H-W, Deng Y, Lawn BR. Brittle fracture versus quasiplasticity in ceramics: A simple predictive index. J Am Ceram Soc 2001;84:561–565.
32. Rudas M, Bush MB, Reimanis IE. The kinking behaviour of a bimaterial interface crack under indentation loading. Eng Anal Bound Elem 2004;28:1455–1462.
33. Qasim T, Bush MB, Hu X, Malament KA, Lawn BR. Margin cracks in brittle dome structures. J Biomed Mater Res B, in press.
34. Tabor D. Hardness of Metals. Oxford: Clarendon; 1951.
35. Zhao H, Hu X, Bush MB, Lawn BR. Cracking of porcelain coatings bonded to metal substrates of different modulus and hardness. J Mater Res 2001;16:1471–1478.